FLIR PAPER — Concentrating on Silicon signal processing with InSb CID's as the 3-5 μm sensor. (See pg. 71)

InSb MIS TECHNOLOGY AND CID DEVICES * (Invited Paper)

J.C. Kim

9:05 – 9:25 presentation
10 min discussion

General Electric Company, Syracuse, New York

Abstract: A metal-insulator-InSb (MIS) technology has been successfully developed; and MIS structures with excellent interface properties can be fabricated. The C-V characteristics of these structures show a completely inverted low-frequency type C-V response at about 10 Hz, an indication of low thermal generation. An analysis of the conductance measurements in the strong inversion region indicates that bulk generation dominates minority carrier thermal generation, leading to good MIS structures.

Conductance techniques were utilized to study the interface properties of these MIS structures leading to a detailed description of the surface state properties. The interface state density of our recent MIS structures is in the range of 10^{11} cm^{-2} eV^{-1}. It appears that the surface states are continuously distributed over the entire InSb bandgap. The experimental results strongly indicate that the InSb MIS interface characteristics are adquately described by the Shockley-Read-Hall treatment model.

These InSb MIS structures have been used as IR sensors operating in the charge injection mode. Their sensitivities approach background-limited performance (BLIP). InSb CID arrays have been fabricated and the results of these array measurements will be discussed.

I. INTRODUCTION

In recent years solid-state imaging devices operating on the basis of a surface charge-coupling principle in the silicon MOS structure have received considerable attention, and considerable progress has been made in both line and large-area imaging devices, with the silicon MOS technology. These devices are used in the visible region of the spectrum. For IR applications a similar approach has been applied to narrow-bandgap semiconductors, namely InSb.

The success of silicon charge-coupled devices is undoubltedly due to the advanced development of the silicon MOS technology, but a suitable dielectric technology for other semiconductors has not yet been fully developed. Most device development work on III-V compound semiconductor has been concerned with p-n junction fabrication and as a result, excellent InSb infrared photovoltaic detectors have been developed. For surface passivation of InSb p-n junction detectors, an anodic

*The early work of this program was supported by the Air Force Avionic Laboratory and Army Night Vision Laboratory. More recent work is being supported by the Naval Research Laboratory and Defense Advanced Research Projects Agency.

oxide of InSb has been commonly used.

A detailed study of anodic oxide InSb MOS structures [1] conducted in our laboratory indicates that majority carrier trapping in the oxide causes the surface state charges. For n-type InSb substrates the majority carrier electrons play the major role in charge trappin in the oxide, resulting in a negative surface state charge. On the other hand, for p-type materials, hole trapping is the dominant mechanism and results in positive surface charges. Both the indium and antimony atoms in anodized InSb oxide, therefore, may be responsible for charge trapping both types of carriers. This variable charge-trapping mechanism leads to an instability of the MOS structure and it is, thus, difficult to use the anodic oxide in MOS devices for stable surface charge-coupling operations.

It was, therefore, necessary that a new dielectric material and a suitable deposition technology be found, if successful InSb MIS surface charge-coupled devices were to be developed. As a result of our recent R&D efforts in this regard, we have found that a dielectric layer of silicon oxynitride (SiON) deposited pyrolytically on an InSb substrate, yields MIS interface properties [2] that allow us to operate the MIS structures as charge injection devices (CID) in the charge storage mode. This paper describes the interface properties of SiON-InSb MIS structure and the experimental results obtained using these structures in the charge injection mode.

II. InSb MIS STRUCTURES

The single crystals of InSb used in this work were grown by the Czochralski method with a (111) orientation. For n-type materials tellurium was used as the dopant with a carrier concentration ranging from $10^{13}/cm^3$ to $10^{16}/cm^3$; for p-type materials cadmium was the dopant at concentrations in the range of $10^{15}/cm^3$. The dislocation densities (EPD/cm^2) of these materials were less than $100/cm^2$.

The large ingots of InSb were cut into wafers about 35 mils thick and 2-4 cm in diameter. After the B face (Sb side) of the wafer was mechanically polished and chemically etched, SiON layers were deposited pyrolytically on the InSb surface. A typical oxide thickness is in the range of 1000Å to 2000Å. The SiON dielectric layer is extremely uniform and pin-hole free.

For a simple InSb MIS structure, a semi-transparent NiCr metal film less than 100Å thick and 20 mils in diameter was vacuum deposited on the SiON layer of InSb wafer. The large wafer was diced into small chips which were, in turn, attached to transistor headers. The device header was mounted in a cryogenic dewar for evaluation.

The MIS structures were measured using a lock-in amplifier or phase-sensitive detection technique. The lock-in amplifier (PAR 124) can be used over a wide range of frequencies and is particularly useful at low frequencies. This admittance bridge permits us to easily measure not only C-V curves but also conductance-voltage characteristics of MIS structure. The conductance of the device can easily be measured by changing the phase angle of the instrument by 90°. The conductance technique was used exclusively to study the interface properties of the structures. All measurements were made at near $77^{\circ}K$, unless otherwise stated.

III. INTERFACE PROPERTIES OF InSb MIS STRUCTURES

1. C-V Characteristics of InSb MIS Structure

The capacitances of the MIS structures were measured as a function of the gate bias voltage at various frequencies, as shown in Figure 1 for an n-type substrate. These measurements were made in the dark condition; that is, the field of view (FOV) was equal to zero. The device could "see" only its own temperature so that no $300^{\circ}K$

photon radiation could have contributed to the minority carrier equilibration process. In this way only the thermal generation process of minority carriers in the device can be determined.

The C-V curves closely follow the simple ideal MIS capacitance model (3). At the positive gate bias the capacitance is approximately that of the insulator; and when the gate is biased negatively, the capacitance is decreased due to the creation of a depletion region on the InSb surface. Further increases in the negative bias cause a strong inversion where the depletion width is fixed, resulting in a minimum capacitance, shown in the high-frequency measurement. Note that the dashed line is a computer-calculated, theoretical C-V curve that follows closely the experimental result, indicating a low surface state density.

To operate this type of device as an optical sensor, e.g. CID and CCD, the strong inversion bias region is important, since the device operates normally here. As the MIS capacitor is biased into the heavy inversion region, it can be shown (4) that the MIS structure results in a simple equivalent circuit; the insulator capacitance (C_o) is in series with the parallel combination of the depletion capacitance (C_D) and a resistor (for the sake of simplicity, we use a conductance, G_g). This simple equivalent circuit can be derived only if the surface state density is relatively small, so that it can be assumed that the surface state capacitance is much smaller than the depletion capacitance. For single-level types of surface states, only those states located near the intrinsic Fermi level contribute significantly to the surface state capacitance, when the Fermi level is near this level; but at the surface of the strong inversion bias the Fermi level is near the top of the valence band (for n-type devices). Therefore, with a relatively low surface state density, the above assumptions are quite valid. Later, it will be shown quantitatively that these assumptions can be applied to our InSb MIS devices.

It has been shown that (5) the change in capacitance in the strong inversion region is due to the relative value of G_g compared to ωC_D. The inversion capacitance changes from the minimum capacitance, $C_o C_D/(C_o + C_D)$, to the maximum insulator capacitance, C_o, as the measurement frequency varies from very high to very low values. Between these two limits the inversion capacitance is a function of frequency and increases with decreasing frequency, as shown in Figure 1.

It has been shown that the capacitance in the strong inversion bias region depends on the relative value of the conductance, G_g. It will be shown later that G_g can be related directly to the thermally generated minority carrier current. If the relaxation rate of the minority carriers is very small in the device, G_g is, indeed, very small and the capacitance results in the high frequency case. This is the case when the minority carrier generation rate cannot keep up with the small signal variation of the capacitance measurement, resulting in a high-frequency type C-V response (equivalent to $\omega C_D \gg G_g$). If, however, the minority carriers can follow the variation in the measurement signal the capacitance rises, approaching the insulator capacitance; this is the low-frequency type of C-V curve, in which case $\omega C_D \ll G_g$. Therefore, the low-frequency C-V data reveal, qualitatively, the minority carrier relaxation rate. The frequency at which the minority carriers completely follow the measurement signal variation is in the range of 10 Hz, indicating that the minority carrier relaxation rate in these devices is, indeed, small.

The interface state density of these MIS devices has been determined quantitatively and it will be shown that the surface state densities are also small.

2. Surface State Density of InSb MIS Structures

Typical conductance (G_m/ω)-voltage characteristics of an n-type InSb MIS

structure at various frequencies are shown in Figure 2. The rise in conductance in certain bias regions is due to the capture and emission process of carriers by the interface states. The sharp single conductance peak is typical of single-level states. If we, therefore, analyze the conductance values in the peak region [6], we can determine the interface state parameters. Since the conductance is caused by the steady-state loss due to the capture and emission of carriers by interface states, this technique is a more direct measure of the interface properties than the use of C-V data.

The conductance technique used here has been described in some detail in reference 2; it provides quite accurate determinations of surface state densities. At each bias point in the peak conductance region, equivalent parallel conductance values were computed from the measured conductance data as a function of frequency. From these conductance curves, then, the surface state densities were obtained for different bias points. The results are shown in Figure 3; the values of surface state density were plotted as a function of surface potential. The circle-dot points represent the values determined by the continuum model, whereas the triangle points were obtained from the single time constant model. It is interesting to point out that, in the depletion region, the experimental points follow the continuum model, whereas, in the weak inversion region, the measured data fit the single time constant model.

As shown in Figure 3, the surface state density varies from mid-10^{10} cm^{-2} eV^{-1} to about mid-10^{11} cm^{-2} eV^{-1}. It is also interesting to note that the interface state density tends to become a minimum near the flatband, which is somewhat different from the silicon case. [6] This result is also evident from the C-V curves shown in Figure 1, where the surface state density in the flatband region appears to be lowest.

The corresponding surface state time constant values were also determined from the equivalent parallel conductance data and measured as a function of the surface potential, as shown in Figure 4. Here, again, the separate data points represent the two models, as indicated. In both cases the time constant varies exponentially with the surface potential, but with different slopes; for the continuum model the slope is $\beta/2$, and for the single time constant case, it is $\beta/4$, where β is q/kT; q is the electronic charge, k is Boltzman's constant, and T is the absolute temperature. The extrapolation of the two lines, however, meets at about the same point in the flatband voltage.

If the capture cross-section is independent of energy then the slope should be equal to β. A slope smaller than β may be due to the fact that the capture cross-section is energy dependent. For the single time constant data, an even slower increase in the time constant may be due to an additional contribution of minority carrier generation.

3. Thermal Generation Mechanism

As shown in Figure 2, in the strong inversion bias region the measured conductance becomes constant and independent of bias, but is a function of the measurement frequency, as in the case of the C-V data. It has been shown that the capacitance variation with frequency in the strong inversion bias region depends on the relative value of G_g with respect to ωC_D. Similarly, the bias-independent conductance values can be used to determine the thermal generation mechanism of these devices.

When an MIS structure with a relatively low interface state density is biased into a strong inversion region, a simple equivalent circuit [4] of the capacitor can be derived; the insulator capacitance (C_o) is in series with the parallel combination of the depletion capacitance (C_D) and a conductance, G_g. For the admittance measurements, the MIS structure is applied with a dc bias, V_g, and a small ac signal, $\Delta V(t)$. The total charge density, Q, is given by

$$Q = Q_p + Q_{sc} \quad (1)$$

where Q_p is the minority carrier charge density in the inversion layer and Q_{sc} is the semiconductor space-charge density. Q_{sc} is then

$$Q_{sc} = qN_D x \,. \tag{2}$$

where N_D is the concentration of the donor impurities and x is the surface depletion depth. The surface potential, ϕ_s, derived from the depletion approximation, is

$$\phi_s = \frac{qN_D x^2}{2\epsilon} \,, \tag{3}$$

where ϵ is the permittivity of InSb.

The time variation of the above quantities can be defined as $Q(t) = Q_o + \Delta Q$, $Q_p(t) = Q_{po} + \Delta Q_p$, $Q_{sc}(t) = Q_{sco} + \Delta Q_{sc}$, $x(t) = x_o + \Delta x$, and $\phi_s(t) = \phi_{so} + \Delta\phi_s$, where Q_o, Q_{po}, Q_{sco}, x_o, and ϕ_{so} are all established by the bias, and ΔQ, ΔQ_p, ΔQ_{sc}, Δx, and $\Delta\phi_s$ are caused by the ac signal and thus are a function of time. Thus, the time dependent quantities are,

$$\Delta Q = \Delta Q_p + \Delta Q_{sc} \tag{4}$$

$$\Delta Q_{sc} = qN_D \Delta x \tag{5}$$

$$\Delta\phi_s = \frac{qN_D x_o \Delta x}{\epsilon} \tag{6}$$

since $x_o >> \Delta x$. The total ac current density, J, can be obtained by differentiating ΔQ with respect to time:

$$J = \frac{d\Delta Q}{dt} = J_p + J_{sc} \,, \tag{7}$$

where $J_p = d\Delta Q_p/dt$, the ac current density charging the inversion layer and $J_{sc} = d\Delta Q_{sc}/dt$, the ac current density charging the depletion layer. J_{sc} can be related to the surface potential by

$$J_{sc} = \frac{d\Delta Q_{sc}}{dt} = \frac{qN_D d\Delta x}{dt} = \frac{\epsilon d\Delta\phi_s}{x_o dt} \tag{8}$$

For a sinusoidal ac signal, $\Delta\phi_s = A \exp(j\omega t)$ and, thus,

$$J_{sc} = j\omega \frac{\epsilon}{x_o} \Delta\phi_s \,. \tag{9}$$

The current density, J_p, that charges the inversion layer, should be equal to the ac current density of minority carrier generation. In general, the minority carrier generation can be divided into three separate generation currents, the surface generation current, the diffusion current outside the space-charge region and the generation current in the space-charge region. For an InSb MIS device operating at 77^oK, the space-charge generation current dominates, as verified later. Assuming that the generation rate in the depletion layer, g, is constant over the space-charge region, the ac generation current density is equal to $qg\Delta x$ (7) and, thus,

$$J_p = qg\Delta x = \frac{\epsilon g}{N_D x_o} \Delta\phi_s \,, \tag{10}$$

from equation (6). It is interesting to note that the ac generation current density depends on x_o, which is established by the dc bias surface potential, ϕ_{so}.

The total ac current density given in equation (7) is simply

$$J = \frac{\epsilon g}{N_D x_o} \Delta\phi_s + j\omega \frac{\epsilon}{x_o} \Delta\phi_s \tag{11}$$

thus, the total ac current ($I = J x A_d$) in the structure of area = A_d is

$$I = Y_{in} \Delta\phi_s \,, \tag{12}$$

where Y_{in} is the admittance of the heavily inverted MIS (on the semiconductor side). Therefore, the equivalent circuit of the structure includes a conductance, G_g, and capacitance, C_D, in parallel. The G_g and C_D are then:

$$G_g = \frac{\epsilon g}{N_D x_o} A_d \tag{13}$$

$$C_D = \frac{\epsilon}{x_o} A_d \,. \tag{14}$$

Note that the conductance, G_g, is directly proportional to the generation rate, g, which, in the space-charge region where both types of carrier densities are small compared to n_i, is directly proportional to the intrinsic carrier density, n_i, [7]

$$g \simeq \frac{n_i}{\tau} , \qquad (15)$$

where τ is the carrier lifetime, it is assumed that the generation centers are located near the intrinsic Fermi level; therefore, G_g should be proportional to n_i in view of Equations (13) and (15), so,

$$G_g \,\alpha\, n_i . \qquad (16)$$

There is experimental evidence for this relation.

For the measurement of G_g the conductance values can be obtained by measuring the terminal conductance of the MIS structure at a fixed bias in the strong region as a function of frequency. Typical measurements are shown in reference (5). Thus, the G_g values are determined by this method as a function of temperature. Figure 5 shows the thermally generated conductance, G_g, as a function of the reciprocal of the absolute temperature; the experimental results yield a straight line on a semi-log plot. The slight departure from a straight line in the low temperature region is due to the noise of the measuring instrument since, in this region, the measurement frequencies used to determine G_g are quite low (less than 100 Hz).

The exponential dependence of G_g on the reciprocal temperature does ensure that the generation mechanism is thermal in nature. Furthermore, from the slope of the straight line, one can see that G_g indeed follows the n_i variation with temperature since

$$n_i \,\alpha\, \exp\left(-E_g/2kT\right), \qquad (17)$$

where E_g is the bandgap energy for InSb and equal to 0.23 ev. The activation energy is correctly equal to $E_g/2$, as shown in Figure 5. Therefore, the dependence of the thermally generated conductance, G_g, on the intrinsic carrier concentration, n_i, indicates that G_g is dominated by generation in the space-charge region of the MIS structure, verifying our earlier assumption. The other generated components are, indeed, smaller than that of the space-charge generation. This means that the minority carrier generation, due to surface state density, does not contribute to the generation mechanism. Therefore, for the inverted InSb MIS structure minority carrier thermal generation is dominated by space-charge generation, which is a bulk generation process, thus leading to good MIS structures.

From Equations (13) and (14), the generation rate, g, is simply given by,

$$g = \frac{G_g N_D}{C_D} , \qquad (18)$$

which can be calculated from the experimentally determined values of G_g and C_D. For an n-type InSb MIS structure ($N_D \simeq 2 \times 10^{15}$ cm, $^{-3}$, $C_o = 72$ pF and $C_{min} = 37$ pF), for example, the depletion capacitance, C_D, and the thermally generated conductance, G_g, are equal to 76 pF and 3.2×10^{-8} mhos, respectively, for a 20-mil diameter device. From these values, the lifetime (τ) can be computed to be approximately equal to 10^{-8} sec, which is well within the range of the reported values [8].

The dark current I_g, generated in the depletion region for the above device is, then, approximately equal to 10^{-8}A and when operated in the charge storage mode, this dark current limits the device's ultimate storage time. The dark current storage time, T_s, can then be related to the dark current [9] as,

$$T_s \simeq \frac{C_o \Delta V}{I_g} , \qquad (19)$$

where ΔV is the voltage swing from inversion to depletion. For $\Delta V = 10\,V$, the dark current storage time is about 0.1 sec. This result is also evident from the C-V data.

It is significant that T_s, here, is roughly seven orders of magnitude greater than the carrier lifetime for InSb MIS devices, which is why the charge storage InSb MIS structure is so attractive as a charge integrating device, even though the carrier lifetime is short. Furthermore, for InSb devices operating in the IR region, the background photon flux that the device sees also generates additional current, which, then, causes a decrease in storage time. Our results [1, 5] indicate that the dark current of these structures is relatively small compared to that generated by the typical background photon flux encountered in the operation. Under this condition the dark current appears to be less important and the background photon-generated current should then determine the device operating storage time.

IV. InSb CID OPERATION USING THE MIS STRUCTURES

The physics of charge injection devices (CID) has been described in some detail [1], and the charge injection mode of operation of InSb MIS structures has been successfully demonstrated. We present here some of the optical measurements obtained on InSb CID devices.

For the signal-to-noise ratio measurements, we used a narrow band spike filter; $\lambda_o = 4.5\ \mu$, peak transmission = 41%, and $\Delta\lambda = 0.2\ \mu$. The input signal radiation through the filter from a blackbody source was computed to be 3.9×10^{-10} watts (peak value). The estimated background photon flux was approximately 10^{13} photons/sec-cm^2.

The conventional sensitivity notation for IR detectors uses D*, given by

$$D^*_{\lambda_o} = \frac{(A_d \Delta f)^{1/2}}{P_s} \frac{V_s}{V_n}, \qquad (20)$$

Measured

where Δf is the bandwidth of the instrument to measure the noise, V_n (volts), and P_s is the input photon signal (watts) to produce the output electric signal, V_s (volts). $D^*_{\lambda_o}$ is equal to $2.8 \times 10^{-8} \times V_s/V_n$, where V_s is the peak-to-peak value. We will compare the measured $D^*_{\lambda_o}$ value of Equation (20) with the best possible theoretical value.

For our results, the best signal was 30 mV (measured at dc and, thus, the peak value) at an integration time of 1 msec. If we operate an array of 32 elements for one msec, the sampling frequency is 3.2×10^4 Hz. For single device measurements, this is the same as a sample pulse period of about 30 μsec, as far as the sampling rate is concerned. Therefore, the noise was measured at this sampling rate, although the signal was measured with a one msec period (= one msec storage time). A wave analyzer with a $\Delta f = 6$ Hz bandwidth was employed to determine the noise values. At the above sampling rate, the measured noise value varies from 3 μv at 100 Hz to 2 μv at 10^4 Hz. We then use an average noise of 2.5 μv in the information bandwidth (= sampling frequency/2) for the measurements.

The signal-to-noise ratio is then,

$$\frac{V_s}{V_n} = \frac{30\ \text{mv}}{2.5\ \mu\text{v}} = 1.2 \times 10^4 . \qquad (21)$$

Substituting Equation (21) in Equation (20), the $D^*_{\lambda_o}$ is,

$$D^*_{\lambda_o} = 3.4 \times 10^{12}\ \text{cm(Hz)}^{1/2}/\text{watt} \qquad (22)$$

The theoretical expression of $D^*_{\lambda_o}$ (BLIP) is given by,

$$D^*_{\lambda_o}\ (\text{BLIP}) = \frac{\lambda_o}{hc} \sqrt{\eta / 2Q_B}, \qquad (23)$$

theoretical

where η is the quantum collection efficiency, Q_B, is the background photon flux and the other quantities are well-known. The collection efficiency, η, for our MIS structures was, generally, equal to 50%. For the above background photon flux level, ($Q_B \simeq 10^{13}$ photons/sec-cm^2), therefore, the theoretical value of the background-limited $D^*_{\lambda_o}$, the best possible sensitivity, is equal to

$$D^*_{\lambda_o} \text{ (BLIP)} = 3.6 \times 10^{12} \text{ cm (Hz)}^{1/2}\text{/watt} \tag{24}$$

which compares closely with the measured value of Equation (22).

In order to measure the device's saturation characteristic, we increased the number of input signal photons and raised the blackbody source temperature to 800°C so that the source signal photons were much larger than the background photons (Q_B). Under this condition, then, the saturation point depends only on the signal photons and can be determined quite accurately. The measured saturation characteristic of a device is shown in Figure 6; the saturation starts at a photon flux density of about 6×10^{14} photons/sec-cm^2. Thus the maximum number of the stored charges with a quantum efficiency of 50% and the integration time of 500 μsec is equal to approximately 3×10^8 carriers.

The above maximum stored charges can be compared with the maximum storage capacity of the MIS capacitor. The stored carrier density, N, in the potential well is given by

$$qN = C_o' (V_g - V_{fb} - \phi_s) - (2qN_D \epsilon \phi_s)^{1/2}, \tag{25}$$

where V_{fb} is the flatband voltage and C_o' is the oxide capacitance per unit area. The maximum stored carrier density, N_{max}, for a given gate voltage, V_g, is determined when the system reaches the steady state, which occurs when the surface potential, ϕ_s, is approximately equal to twice the bulk potential, ϕ_F; $\phi_s \simeq 2\phi_F$. Thus, N_{max} is

$$qN_{max} \simeq C_o'(V_g - V_{fb} - 2\phi_F) - (4qN_D \epsilon \phi_F)^{1/2} \tag{26}$$

For the device used, $C_o' = 3.2 \times 10^{-8}$ F/cm^2, $V_g - V_{fb} - 2\phi_F \simeq 2$ volts and $N_D \simeq 10^{16}$cm^3. Since the bulk Fermi level of n-type InSb at this doping level is near the conduction band, the bulk potential, ϕ_F, is equal to about 0.1 volts. Using these values, the maximum carrier density, N_{max}, that can be stored in the MIS structure is,

$$N_{max} \simeq 2 \times 10^{11} \text{ carriers/cm}^2, \tag{27}$$

which leads to the maximum number of stored carriers for an area of 2×10^3 cm^2, i.e. 4×10^8 carriers. This value agrees with the experimentally determined value of 3×10^8 carriers within the experimental accuracy.

As shown in the above equation, N_{max} is directly proportional to the gate voltage, V_g. To increase the storage capacity, however, V_g cannot be increased to any arbitrary higher value, because the avalanche breakdown voltage of InSb materials appears to be relatively small. It should be pointed out, however, that the measured dynamic range for $\Delta f = 6$ Hz is already in the range of six orders of magnitude.

The spectral response of InSb CID devices was also measured; the results are shown in Figure 7. For these measurements an integration time of 100 μs was used. The device output signal voltage, corrected for the thermocouple readings, was measured as a function of wavelength.

It is interesting to note that there is no sharp peak in the spectral response and that the response in the shorter wavelength region is excellent. In fact, the quantum

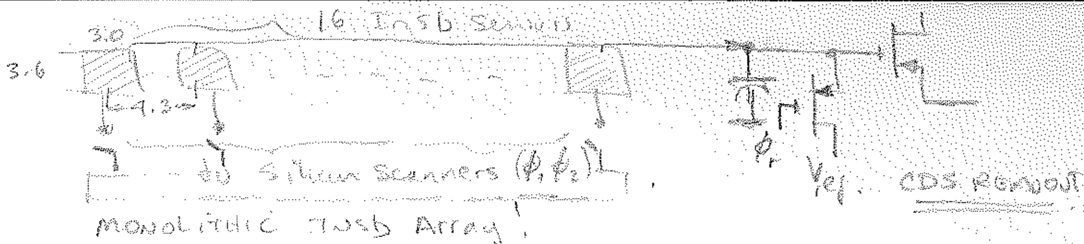

efficiency is almost constant from 5μ to 1μ. This is due to the fact that, for such a device structure, high collection efficiencies can be obtained since the depletion region is formed at the surface. No carrier diffusion is required for collection, as is normally required in a p-n junction photodiode, because most of the carriers are generated in the high field region. This is why, for the higher energy photons (shorter wavelength region), the quantum efficiency is as good as that for the peak response.

V. CONCLUSIONS

A metal-insulator-InSb MIS technology has been developed. The interface state density of these structures conforms to the Shockley-Read-Hall theory of interface states; experimentally the density has been measured in the range of 10^{11} cm^{-2} eV^{-1} (varying with the surface potential from the mid-10^{10} to mid-10^{11} cm^{-2} eV^{-1} range).

Because of the low surface state densities, we have been able to fabricate InSb MIS structures that operate in the charge injection mode. The quality of the interface of these devices makes possible low dark currents, near background-limited performance, and a saturation characteristic that follows the theoretically expected storage capacity of an MIS capacitor. A detailed analysis of the interface properties based on conductance measurements agreed well with theoretical models.

ACKNOWLEDGEMENT

The author would like to thank Messrs. W.E. Davern, T. Shepelavy and Mrs. V.F. Meikleham, for their device processing and fabrication work, and Mr. J.M. Hooker for his valuable technical discussions on measurement circuitry.

BIBLIOGRAPHY

1. J.C. Kim, "Infrared Detector Mosaic Development", Technical Report AFAL-TR-73-352, August 1973.
2. J.C. Kim, "InSb MOS Detector", Final Technical Report, Army Night Vision Laboratory, Contract No. DAAK02-73-C-0006, February 1975.
3. A.S. Grove, F.H. Snow, B.E. Deal, and C.T. Sah, "Simple Physical Model for the Space-Charge Capacitance of Metal-Oxide-Semiconductor Structures", J. Appl. Phys., Vol. 35, pp. 2458-2460, 1964.
4. S.R. Hofstein and G. Warfield, "Physical Limitations on the Frequency Response of a Semiconductor Surface Inversion Layer", Solid State Electronics, Vol. 8, 321, 1965.
5. J.C. Kim, "Interface Properties of InSb MIS Structures", IEEE Tran. Parts, Hybrids, and Packag. (Special Issue on Materials), Vol. PHP-10, pp 200-207, Dec. 1974.
6. E.H. Nicollian and A. Goetzberger, "The Si-SiO_2 Interface-Electrical Properties as Determined by the Metal-Insulator-Silicon Conductance Technique", Bell System Technical Journal, Vol. XLVI, No. 6, 1055, 1967.
7. C.T. Sah, R.N. Noyce, and W. Shockley, "Carrier Generation and Recombination in P-N Junctions and P-N Junction Characteristics", Proc. IRE, Vol. 45, pp. 1228-1243, 1957.
8. R.A. Laff and H.Y. Fan, "Carrier Lifetime in Indium Antimonide", Phys. Rev., Vol. 121, pp. 53-62, 1961.

Summary

N_{ss} = mid 10^{10} cm^{-2} eV^{-1}
BLIP Limited Performance
2-D arrays demonstrated.

(1) has not measured uniformity in InSb Arrays!
(2) has not examined optical cross-talk.

9. G.F. Amelio, W.J. Bertram, Jr., and M.F. Tompsett, "Charge-Coupled Imaging Devices: Design Considerations", IEEE Trans. on Electron Devices, Vol. ED-18, pp. 986-992, 1971.

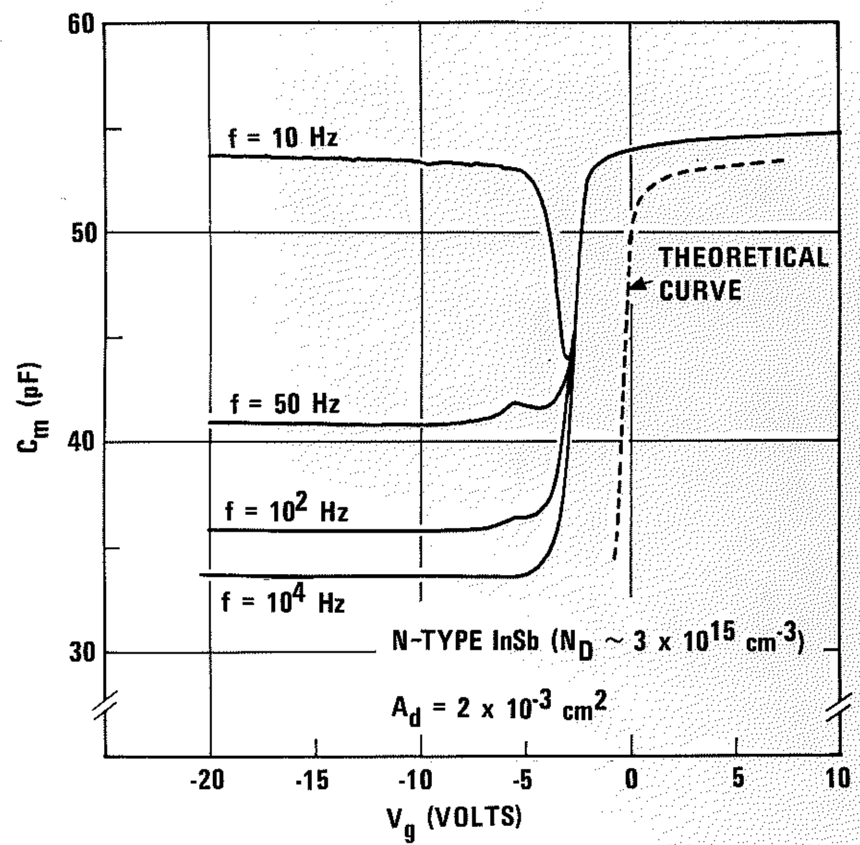

Figure 1. C-V Characteristics of InSb MIS Structure

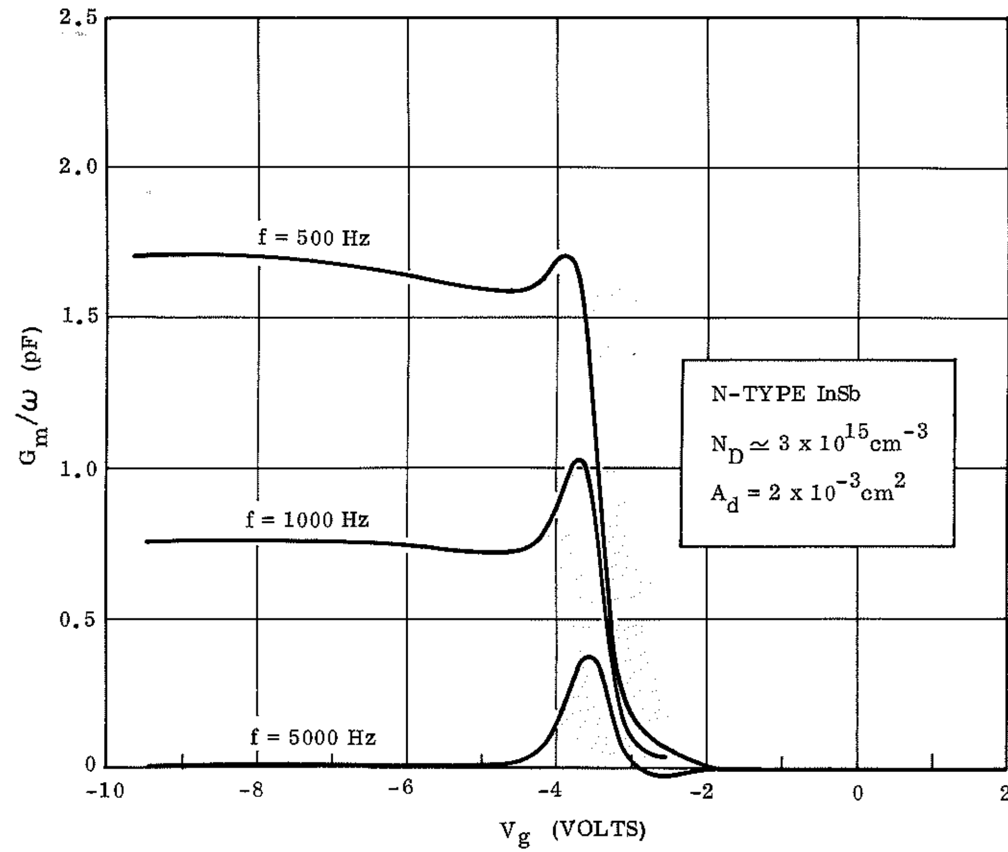

Figure 2. G_m/ω - Voltage Characteristics of InSb MIS Structure.

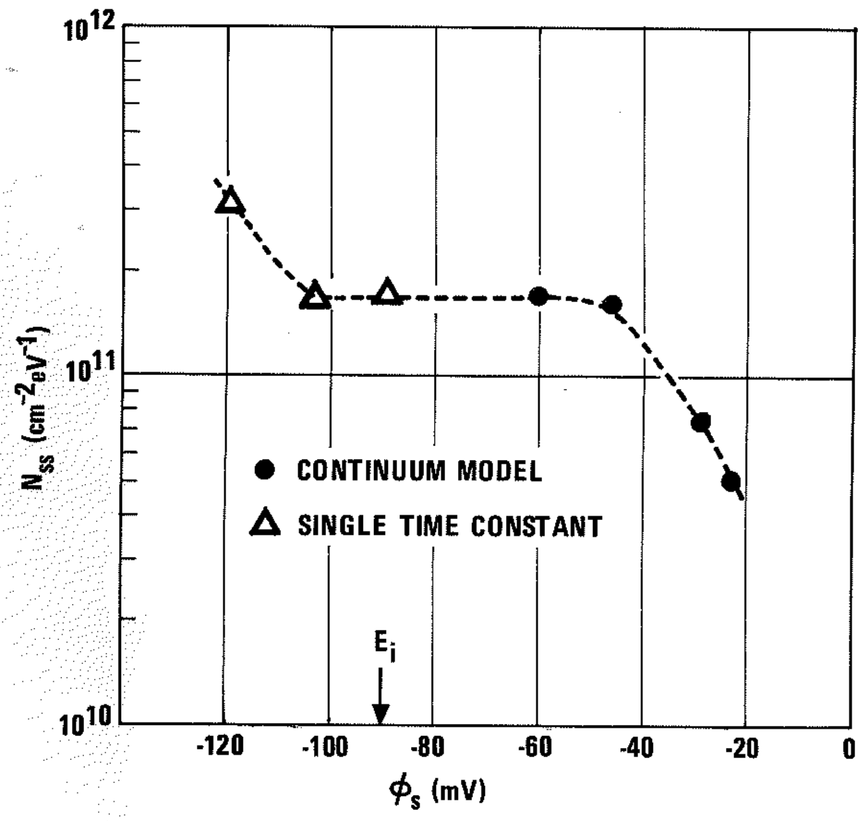

Figure 3. Surface State Density (N_{SS}) vs Surface Potential (ϕ_S).

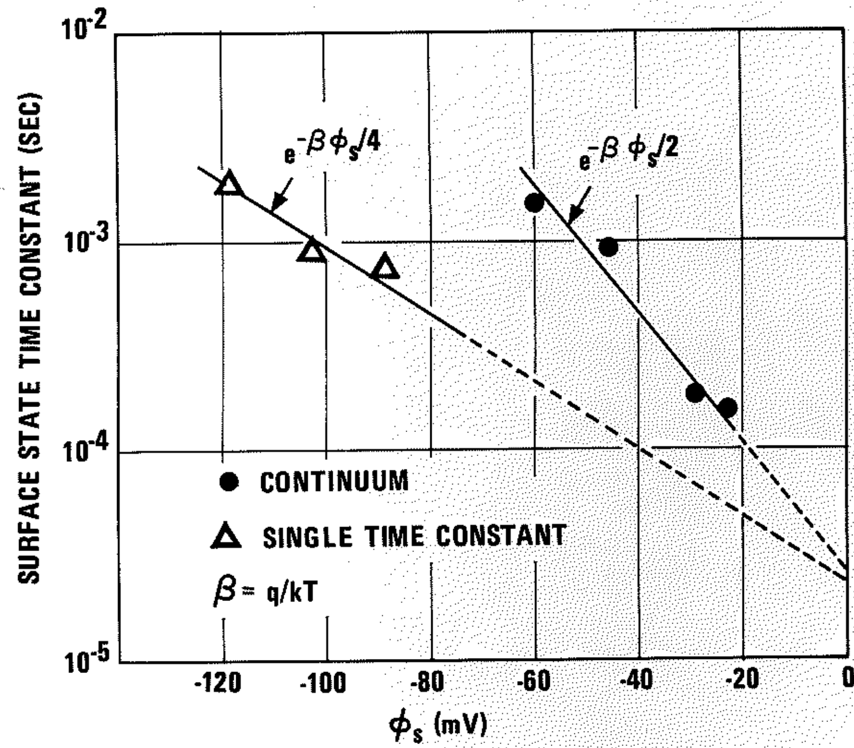

Figure 4. Surface State Time Constant vs Surface Potential.

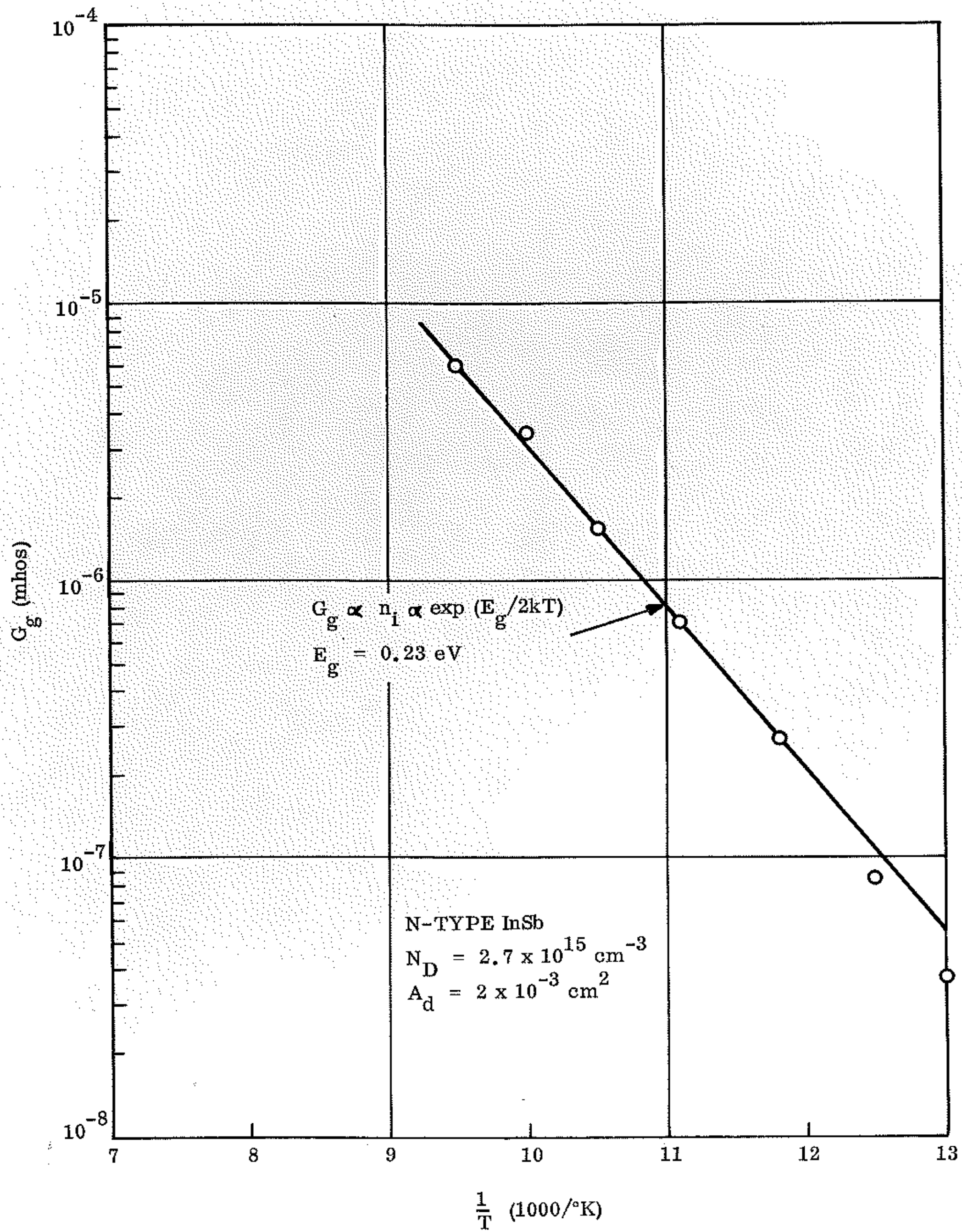

Figure 5. Thermally Generated Conductance (G_g) vs Reciprocal Temperature (1/T).

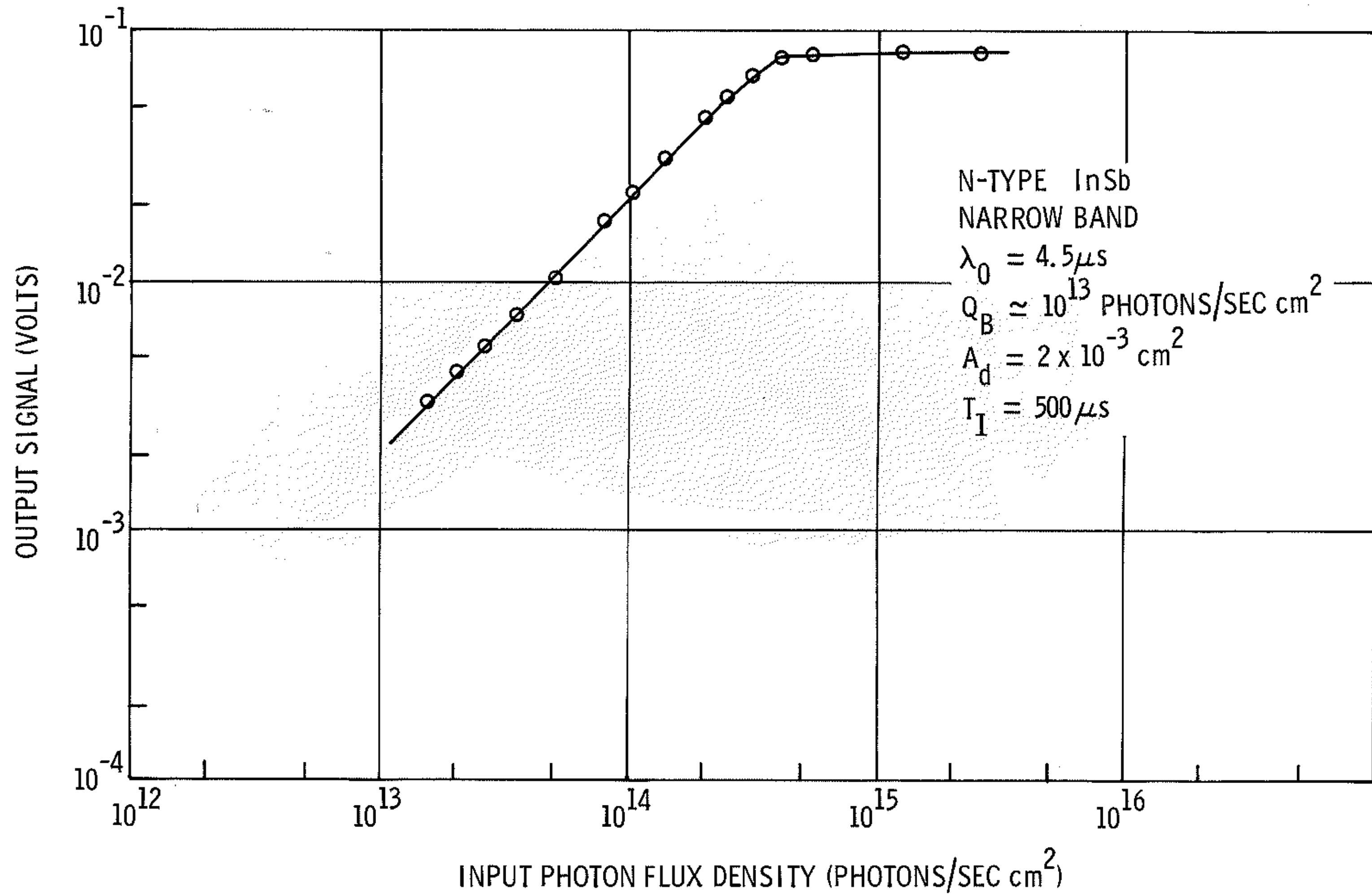

Figure 6. Saturation Characteristic of N-type InSb CID ($N_D \simeq 10^{15}$ cm^{-3}) Measured with a Narrow Spectral Filter

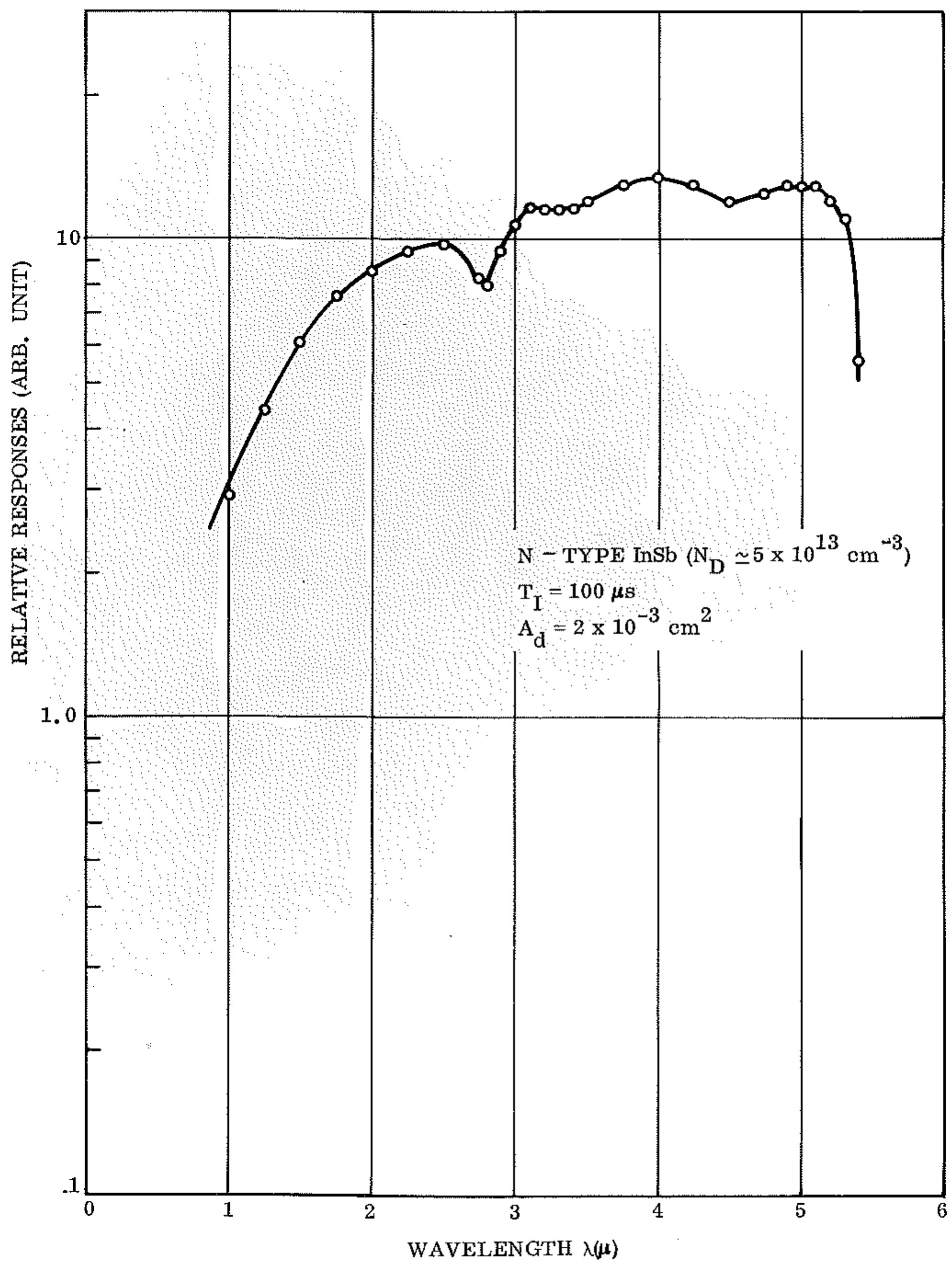

Figure 7. Spectral Response of N-type InSb CID ($N_D \simeq 5 \times 10^{13}$ cm^{-3}).